IRIS MARINER 9 DATA REVISITED : 1) - AN INSTRUMENTAL EFFECT

By

V.Formisano(1,*) , D. Grassi(1) , and G. Piccioni(2),
J.Pearl (3), R. Hanel (4), G. Bjoraker (3), B. Conrath (5)

1. IFSI – CNR, Area Tor Vergata , Roma, Italy.
2. IAS – CNR, Area Tor Vergata, Roma, Italy.
3. Goddard Space Flight Center, Greenbelt, MD, USA.
4. Ann Arbor, MI, USA.
5. Cornell University, Ithaca, NY, USA.

Abstract

Small spurious features are present in data from the Mariner 9 Infrared Interferometer Spectrometer (IRIS). These represent a low amplitude replication of the spectrum with a doubled wavenumber scale. This replication arises principally from an internal reflection of the interferogram at the input window. An algorithm is provided to correct for the effect, which is at the 2% level. We believe that the small error in the uncorrected spectra does not materially affect previous results; however, it may be significant for some future studies at short wavelengths. The IRIS spectra are also affected by a coding error in the original calibration that results in only positive radiances. This reduces the effectiveness of averaging spectra to improve the signal to noise ratio at small signal levels.

Keywords:

IRIS Mariner 9 instrument, Fourier spectrometry.

(*) corresponding author.
E-mail: formisan@nike.ifsi.rm.cnr.it
Phone: +39-6-49934362
Fax: +39-6-49934383

Introduction

On November 14, 1971, the Mariner 9 spacecraft entered martian orbit. During its one year lifetime, it provided the first long term, high resolution monitoring of the planet. One of the most challenging investigations used an infrared interferometer spectrometer (IRIS). This Fourier spectrometer covered the spectral range 5 – 50 μm (200 – 2000 cm^{-1}) at an apodized resolution of 2.4 cm^{-1} (Hanel, et al., 1972). The scientific objectives of the IRIS included studies of the composition, abundance, and distribution of atmospheric gases and aerosols. The detailed measurement of the CO_2 15 μm band enabled the determination of atmospheric pressure-temperature profiles, from which the wind field, and many aspects of atmospheric dynamics could be inferred. Rotational water vapor lines permitted the determination of atmospheric water vapor content. Additional early results included first estimates of the dust aerosol composition, the identification of water ice clouds, the identification of CO_2 in the residual south polar cap, upper limits on many atmospheric gases, and determination of the carbon and oxygen isotopic composition of the atmosphere (Hanel, et al., 1972 a, b, c; Conrath, et al., 1973; Curran, et al., 1973; Maguire, 1977). The achievement of the IRIS scientific objectives, as well as others, unforeseen, provided a new demonstration of the power of Fourier spectrometry for planetary studies.

The information collected in the IRIS data, however, is still not completely exploited. Even today, investigators return to this dataset to confirm or complement other observations, or to find new results. In our case the reasons for revisiting the IRIS data are twofold: 1) from the IRIS investigation we want to learn about the problems that a Fourier spectrometer may generate, and 2) from the data analysis we want to develop the complex software needed to derive the vertical temperature profile of the atmosphere from the 15 μm CO_2 absorption band. This is motivated because some of us (V.F., D.G., G.P.) are presently building the Planetary Fourier Spectrometer (PFS) for ESA's Mars Express mission. This instrument will have two channels: a Long Wavelength (LW) channel covering the wavelength range 5 – 45 μm, with an apodized spectral resolution of 2 cm^{-1} (and therefore very close to the IRIS instrument) , and a Short Wavelength (SW) channel that covers the wavelength range 1.2 – 5 μm, also with a spectral resolution of 2 cm^{-1}. It is clear that we can learn a great deal from the IRIS investigation, and it has been with this spirit that we have been studying IRIS data.

An early result of our studies was the recognition of an instrumental effect, not reported in the literature, which does not essentially change previously published results, but that may become important for future studies. Indeed, once the instrumental effect has been corrected, new interesting information can still be obtained from data acquired so long ago. Here we report the instrumental effect and its probable cause, and present a correction procedure. Future papers shall present scientific results obtained from IRIS data after correction for this effect has been made.

The IRIS data set

IRIS took 21 167 calibrated infrared spectra of Mars. The calibration procedure used two reference black bodies: an internal black body maintained at 254K, and the 3K blackbody radiation of deep space (Hanel, et al., 1972 b; Hanel, et al., 1992). The derived noise equivalent spectral radiance was of the order of 5 10^{-8} W cm^{-2} sr^{-1}/cm^{-1}. The angular diameter of the instantaneous field of view was 4.5 degrees. For nadir viewing at pericenter (nominally near 1400 km) this gave a footprint diameter of 110 km; observations were taken to altitudes of 11000 km. The available IRIS dataset comprises absolute calibrated radiances. Each IRIS spectrum is accompanied by a header that contains a number of important parameters, including spacecraft clock time (DAS), Latitude, Longitude, solar areocentric longitude (L_s), altitude above the planet, incidence angle of the observation, local time of the observation, and a number of other parameters.

The Mariner 9 spacecraft arrived at Mars at $L_s = 293°$, during a global dust storm that covered the planet for several months. By the end of the primary mission at $L_s = 345°$ the dust had cleared

considerably, but many of the IRIS spectra still contained the strong spectral signature of atmospheric dust, which generates a broad absorption band from 200 to 1250 cm^{-1}. For the investigations below, we use the strongest portion of this band to classify the IRIS spectra in the following way.

First, for each observation we estimated the surface temperature by fitting a Planck function to the spectrum in the range 1500- 2000 cm^{-1}. Clearly, this assumes that in this interval the surface emissivity equals one, and that the signal is significantly above the noise. The latter is not always true, so many spectra were not included in the study; such spectra are considered later. Once the temperature of the "martian surface" was known, we introduced a band depth parameter, D, which was computed as follows:

$$D = 100 \cdot \left(\frac{\sum_{j=1}^{N} \frac{I(\nu_j)}{B(\nu_j, T_{ground})}}{N} - 1 \right)$$

where $I(\nu_j)$ is the measured spectrum at the j-th sampling point and $B(\nu_j, T_{ground})$ is a Planck function with the temperature equal to the temperature of the Martian surface. The summation spans over the wavenumebr range [1050;1150] cm^{-1}. Here we can find N=85 IRIS sampling points. The parameter D is related to the dust opacity of the atmosphere and to the thermal contrast between the dust aerosol and the surface. In this study, however, it is only considered as a useful indicator of dust band depth.

Spectra were averaged on the basis of their values of D. Five intervals of D were chosen: [-5; 5], [5; 15], [15; 25], [25; 35], [35; 100]. The high signal to noise ratio in the resulting five averages allowed us to study extremely weak features. We excluded from the averaging all spectra with ground temperature lower than 180 K because we were not able to define the Planck function needed to compute the parameter D.

It can be argued that the physical interpretation of averages constructed in this way is obscure. However, for the present application, this is of no consequence, as we are interested in assessing only the character of the spectra as related to the performance of the IRIS instrument. Nonetheless, as a check on the results presented below, we also considered average spectra computed by using the black body temperature as a binning parameter, rather than the parameter D; the results found were the same.

The instrumental effect seen in the data

In a study of the isotopic composition of C and O in the Martian atmosphere, Maguire (1977) used a spectrum that was the average of 1747 single measurements. Although nearly all of the spectral features were identified as due to CO_2, H_2O or dust, five features were pointed out as of unknown origin, and as occurring "at nearly twice the wavenumber of a corresponding band in the 15-μm region of CO_2." Those lines are clear evidence of an instrumental effect which we describe below in more detail.

In Figure 1 we display the average of the 2656 IRIS spectra that satisfy the condition: $-5 < D < 5$. These spectra represent conditions of low atmospheric dust, of low thermal contrast between the atmospheric dust and the surface, or some combination of the two. We note the presence of the strong 15 μm (668 cm^{-1}) CO_2 absorption band in the average spectrum. We also note that the noise in this spectrum is very low, so that almost all of the small features seen in the figure are real. The most striking characteristic of the spectrum, after the 668 cm^{-1} band, is a well defined absorption band centered at 1336 cm^{-1}= (668 · 2) cm^{-1}. The 15 μm band has a number of satellite Q branches;

eight of these satellites are visible in Figure 1. They appear as narrow absorption lines at 545, 597, 617, 643, 669, 719, 740 and 792 cm^{-1}.

The correspondence of the structures near 668 cm^{-1} and 1336 cm^{-1} is illustrated in Figure 2. Two parts of the spectrum plotted in Figure 1 are shown. The upper panel gives the normal 15 μm CO_2 absorption band, while the lower shows its "ghost" at 1336 cm^{-1}. In order to emphasize the similarity of the "ghost" band with the 15 μm CO_2 band, the wavenumber range in the lower panel is twice that in the upper, and the vertical scale in the lower panel has been expanded. At least 5 ghosts of Q branch lines are now clearly visible in the lower panel, and the ghost band itself has the same shape as the 668 cm^{-1} band.

In order to verify that this effect is not an artifact of using spectra that have a negligible dust absorption band, but is a general effect in the IRIS data, we investigated the remaining large averages. Averages with successively larger values of D show progressively stronger dust absorption features. The average of spectra for which $5 < D < 15$, containing 6566 observations, is shown in Figure 3.

The spectrum is very similar to that in Figure 1. Once again we see the ghost of the 668 cm^{-1} CO_2 band at 1336 cm^{-1}. Because aerosol absorption bands are now also present (as seen prominently between 800 and 1200 cm^{-1}), the ghost band is somewhat distorted, as it is superimposed on some of these features.

An illustration of the doubling effect under conditions of reversed contrast is shown in Figure 4. This is an average of 100 spectra taken during the northern winter and spring seasons at mid – high latitudes. These spectra were too cold to be included in the averages based on D values. Here, the very cold surface and warm atmosphere result in the appearance of the 15 μm CO_2 band in emission; a ghost of this band is present in emission above the noise level.

The appearance of this ghost on a steeply rising continuum deserves discussion. In the calibration of the IRIS data, a coding error was made that resulted in the production of only positive radiances. For signals greater than approximately three times the instrument noise equivalent spectral radiance (NESR), this has no effect on the calibrated spectrum. Very small signals, however, no longer contain a gaussian noise component with standard deviation given by the NESR because the sum of signal plus noise is constrained to be positive. Thus, the averaging of spectra in regions of low intrinsic signal no longer reduces the noise by roughly the square root of the number of spectra averaged. In fact, in the limit of zero intrinsic signal, a large average converges to a positive 'signal' equal to 0.68 times the NESR. This is the source of the spurious, nearly linear brightness temperature trend above 1400 cm^{-1} in Figure 4. If the intrinsic signal is more than 2 or 3 times the NESR, the average will not be affected by this error. In Figure 4, this condition is reached near 1100 cm^{-1}.

Careful inspection of all five of our large averages shows that:

1) The ghost of the 15 μm CO_2 band and its Q branches appears independently of the amount of dust in the spectra, i.e., for all values of D;
2) Additional lines of CO_2 also have ghosts. In particular, lines at 596, 605, 617, 710, 720, and 740 cm^{-1} have low amplitude ghosts at 1192, 1212, 1234, 1420, 1440, and 1480 cm^{-1}; within the IRIS sampling interval of 1.17 cm^{-1}, each of the ghost positions is twice that of its primary line;
3) The intensities of the ghost lines consistently follow the relative intensities of their primary lines at the level of 2-5% (most of the variability is due to the difficulty of precisely determining these small values). We have also looked for ghosts of rotational water vapor lines at low wavenumbers (<300 cm^{-1}). These lines are much weaker than the CO_2 Q branches, and the ghost positions fall among other existing water and CO_2 lines. We find that ghosts of these lines, if present, must also have amplitudes of no more than a few percent of the primary line.

We conclude that the IRIS spectral data contain a spurious component that is related to a frequency-doubled replication of the input spectrum. The ghost intensity of resolved spectral features is of the order of a few percent of the main features, and is essentially independent of wavenumber.

It should be kept in mind that the ghosts are more highly dispersed than the real lines; therefore the lines appear deeper in the ghosts than in the normal spectrum. In this sense the intensity ratio, which ranges from 2-5%, should not be considered a measurement of the intensity of the extra radiation causing the ghost features. As was mentioned previously, and is evident from the figures, the measurement of the ghost line intensity is often very difficult, because of the presence of other real features (as in the region below 400 cm^{-1} which contains the rotational water lines), or because the continuum is changing rapidly. In any case the effect is probably essentially constant, and of a value of a few percent.

Explanation of the instrumental effect

The Mariner 9 IRIS instrument is described in Hanel, et al. (1972) and Hanel, et al. (1992). The instrument follows the classical Michelson scheme (for a more detailed description see Figure 5.8.2 of Hanel, et al., 1992). We shall indicate with letters the optical elements of the instrument. We have the entrance window/filter "e", the beam splitter "s", the fixed mirror "a", the moving mirror "b", and the parabolic collecting mirror "c". The instrumental effect was generated by the element "e" acting as a partially reflecting mirror. It is assumed here that the entrance window was normal to the optical axis (rather than tilted), although the precise optical alignment is not known. Together with an imperfect antireflection coating on the element, this can result in a partial reflection of the outgoing interferogram back into the interferometer (see Chapter 5.6.b of Hanel, et al., 1992).
To study the consequences of such an arrangement, let us indicate each spectral component of the martian radiation entering the instrument by I, and label the path within the interferometer by the sequence of optical elements engaged. Then to second order, the following beams will be incident on the parabolic collecting mirror "c":

$$I_{Tot} = [I_{esasc} + I_{esbsc}] \; + \; [k(I_{esasesbsc} + I_{esbsesasc})] \; + \; [k(I_{esasesasc} + I_{esbsesbsc})]$$

Here k is a small fraction of the radiation returned to the interferometer from the entrance window "e". Of the six beams going to the collecting mirror, the first two produce the normal interferogram. They undergo an optical path difference δ that is determined by the motion of the mirror "b". The second two beams always have zero optical path difference, so they contribute only to a background continuum and do not affect the spectrum. The last two beams have optical path difference 2δ because the first has gone twice to the fixed mirror, and the second has gone twice to the moving mirror. Consequently, the interferogram absorbed at the detector consists of a principal part with optical path difference δ and a secondary part with optical path difference 2δ. This superposition will result in a spectrum containing a ghost of the main spectrum, with all features appearing at twice the frequency, but with an intensity determined by the value of k.
However, reflection from the inside surface of the entrance window is not the only source of ghosts. Internal reflection from the outside surface and reflection from the detector may produce similar effects. The contribution from the detector is expected to be the smallest, not only because it was manufactured to be as absorbing as possible, but because it also has a rough unpolished surface. Consequently, it scatters the small amount of reflected radiation over a large solid angle. Without detailed knowledge of the detector properties and of the antireflection coatings on the entrance window, it is not possible to precisely specify the contributions of the three reflecting surfaces to the ghost spectrum. We therefore combine their effects into an empirically determined parameter, β, as derived below.

Recalibration of the data

The IRIS data tapes cannot be located. Consequently the phase information that was in the original interferograms has been lost, and is not available to us for use in recalibration. However, by investigating the calibration method, we can devise a procedure to correct the existing spectra.
The IRIS data were calibrated by using two blackbodies (see Chapter 5.13.b of Hanel, et al., 1992): an internal blackbody at temperature T_{warm}, and deep space as a cold black body at T_{cold}=3K. At each wavenumber, ν, the measured signal amplitudes, A, while observing Mars and the two blackbodies are, respectively:

$$\begin{aligned} A_{mars} &= R(\nu) \cdot (I_{mars} - B(\nu, T_{instr})) \\ A_{warm} &= R(\nu) \cdot (B(\nu, T_{warm}) - B(\nu, T_{instr})) \\ A_{cold} &= R(\nu) \cdot (B(\nu, T_{cold}) - B(\nu, T_{instr})), \end{aligned} \qquad (1)$$

where $R(\nu)$ is the instrument responsivity, I_{mars} is the martian spectrum, $B(\nu,T)$ is the Planck function for temperature T, and T_{inst} is the instrument temperature.
By assuming negligable radiation from the deep space black body, the responsivity of the instrument can be eliminated to give the standard calibration relation:

$$I_{mars}(\nu) = B(\nu,T_{warm}) \cdot \frac{A_{mars} - A_{cold}}{A_{warm} - A_{cold}} \qquad (2)$$

If a small additional component of magnitude β results from reflection within the instrument (and, hence, has a wavenumber dependence ν/2), then a first order adjustment to the calibration can be derived by expanding each of the above quantities, and retaining terms through order β. This results in:

$$I_{mars}(\nu) = I_{0mars}(\nu) - \beta \cdot I_{0mars}(\nu/2) + \beta \cdot I_{0mars}(\nu) \cdot \frac{B(\nu/2,T_{warm})}{B(\nu,T_{warm}),} \qquad (3)$$

where:

$$I_{0mars}(\nu) = B(\nu,T_{warm}) \cdot \frac{A_{mars} - A_{cold}}{A_{warm} - A_{cold},} \qquad (4)$$

This shows that the ghost spectrum contains contributions from the spectrum of the warm blackbody, as well as from the martian spectrum itself. In addition, because the instrument passband cuts off below 200 cm^{-1}, no adjustment occurs for wavenumbers below 400 cm^{-1}.
Equations 3 and 4 provide the basis for a first order correction to the IRIS spectra. Equation 4 was applied to the original interferograms to produce the existing spectra. Since β is small, each spectrum, $I_{0mars}(\nu)$, can be used in Equation 3 to create a corrected spectrum, $I_{mars}(\nu)$.
A consequence of this recalibration technique is a gradual rolloff of the spectra to higher wavenumbers. A similar small effect is present in many of the martian spectra collected by the Thermal Emission Spectrometer experiment on the orbiting Mars Global Surveyor spacecraft. It also appears in some of the Mariner 7 Infrared Spectrometer data (Cimino and Calvin, 1996; Kirkland, 1999).
By using a large average of IRIS spectra as I_{0mars}, and assuming that β is independent of wavenumber, we have found empirically that β=0.023 eliminates the ghost Q branches near 1336 cm^{-1}. This is shown in Figure 5, which also shows the sensitivity of the spectrum to this parameter. The features near 1235 and 1440 cm^{-1} are most diagnostic for establishing β. We note that the adjustment is precise enough to reveal a significant water vapor line on the low wavenumber side of

the 1440 cm^{-1} feature. As can be seen from the figure, the slope of the high wavenumber rolloff is extremely sensitive to the value of β.
With the value of β in hand, the IRIS spectra may be corrected individually for the ghosts. It is clear from the corrected spectra of Figures 1 and 3 that the adjustment is important mostly above 1000 cm^{-1}. This range has not been used much in scientific research involving IRIS data in the past, but is a region where important potential surface minerals have characteristic absorption features. Therefore the correction of this instrumental effect may generate new results, while, at the same time not materially affecting most previously published results based on IRIS data. The correction suggested here should be important only when either the wavelength range above 1000 cm^{-1} is being investigated, or in special cases when small features are being studied which could be confused with ghosts of other features at lower wavenumbers.

Discussion and Conclusions

An instrumental effect has been found in the IRIS data that results in a small amplitude replication of the spectrum with a doubled wavenumber scale. It is due to weak reflections of exiting radiation at the entrance window, and possibly at the detector. A method is given to correct for the phenomenon. The best estimate for the amplitude of the effect is about 2%. Most of the results published in the past are not materially affected by this adjustment. However, for studies involving short wavelengths, where the correction is most significant, new interesting results may be forthcoming from the IRIS data, as shown, for example, by a study of the aerosol dust composition in the martian atmosphere (Grassi and Formisano, 1999).

References

Cimino, G., and Calvin, W.M., *Calibration and Analysis of Mariner 7 Infrared Spectra,* Bull. Am. Astron. Soc., 28, 1068, 1996.

Conrath, B.; Curran, R.; Hanel, R.; Kunde, V.; Maguire, W.; Pearl, J.; Pirraglia, J.; Welker, J. *Atmospheric and surface properties of Mars obtained by infrared spectroscopy on Mariner 9,* Journal of Geophysical Research, vol. 78, p. 4267-4278, 1973

Curran, R.J., Conrath, B.J., Hanel, R.A., Kunde, V.G., Pearl, J.C., *Mars: Mariner 9 spectroscopic evidence for H_2O ice clouds,* Science, 175, pag. .381-383, 1973

Grassi D. and Formisano, V. *: IRIS Mariner 9 data revisited : Aerosol dust composition .* Submitted *to Planetary and Space Science*, 1999.

Hanel, R. A.; Schlachman, B.; Breihan, E.; Bywaters, R.; Chapman, F.; Rhodes, M.; Rodgers, D.; Vanous, D., *Mariner 9 Michelson interferometer*, Applied Optics, no.11, pag. .2625-2634,1972a

Hanel, R.; Conrath, B.; Hovis, W.; Kunde, V.; Lowman, P.; Pearl, J.; Prabhakara, C.; Schlachman, B.,, *Infrared spectroscopy experiment on the Mariner 9 mission: preliminary results*, Science, vol.175, pag. 305-308, 1972b

Hanel, R.; Conrath, B.; Hovis, W.; Kunde, V.; Lowman, P.; Maguire, W.; Pearl, J.; Pirraglia, J.; Prabhakara, C.; Schlachman, B., *Investigation of the Martian environment by infrared spectroscopy on Mariner 9*, Icarus, vol.17, pag. 423-442, 1972c

Hanel, R.A., Conrath, B.J., Jennings, D.E., Samuelson, R.E., *Exploration of the Solar System by infrared remote sensing*, Cambridge University Press, 1992

Kirkland, L. *Infrared Spectroscopy of Mars,* Dissertation, Rice University, Houston, TX, 1999.

Maguire, W.C., *Martian isotopic ratios and upper limits for possible minor constituents as derived from Mariner 9 infrared spectrometer data*, Icarus, no.32, pag. 85-97, 1977

Figures captions

FIG. 1 – Average of IRIS spectra that show negligible thermal contrast in the dust band. The upper curve is the uncorrected spectrum; the lower gives the corrected spectrum (between 400 and 1700 cm^{-1}) according to the procedure described in the text. Oblique lines represent the brightness temperature equivalent to instrumental 0.68·NESR (right) and 3·NESR (left).

FIG. 2 – Portions of the average spectrum shown in Fig. 1, but expanded around the 668 cm^{-1} and the 1336 cm^{-1} features to show the principal band (upper panel) and its ghost (lower panel).

FIG. 3 – IRIS average spectrum with some dust present. Again, the upper curve gives the uncorrected spectrum, and the lower curve the spectrum corrected for the instrumental effect, as described in the text. Diagonal lines have the same meaning as in Figure 1.

FIG. 4 – IRIS average spectrum for very low ground temperatures. The oblique line in the figure represents a continuum defined by 0.68 times the NESR of the instrument. The inserted panel is an expanded view of the ghost band with the continuum removed.

FIG. 5 – The empirical determination of the parameter β, and the sensitivity of ghost amplitudes to its value. The solid line represents the unadjusted spectrum, the dotted line the spectrum adjusted using β=0.02, and the dashed line the spectrum adjusted using β=0.04. The unadjusted spectrum is an average of 1622 IRIS spectra selected to have brightness temperatures at 1300 cm^{-1} between 260K and 290K. The lines at 1193, 1235, 1336 and 1440 cm^{-1} are ghosts of Q branches in the 15 μm CO_2 band, while the broad region between 1240 and 1400 cm^{-1} contains the ghost of the band itself. A value of β close to 0.02 most satisfactorily cancels the ghost lines. The mineralogically important spectral region 1240-1400 cm^{-1} and beyond is very sensitive to this parameter.

Figures

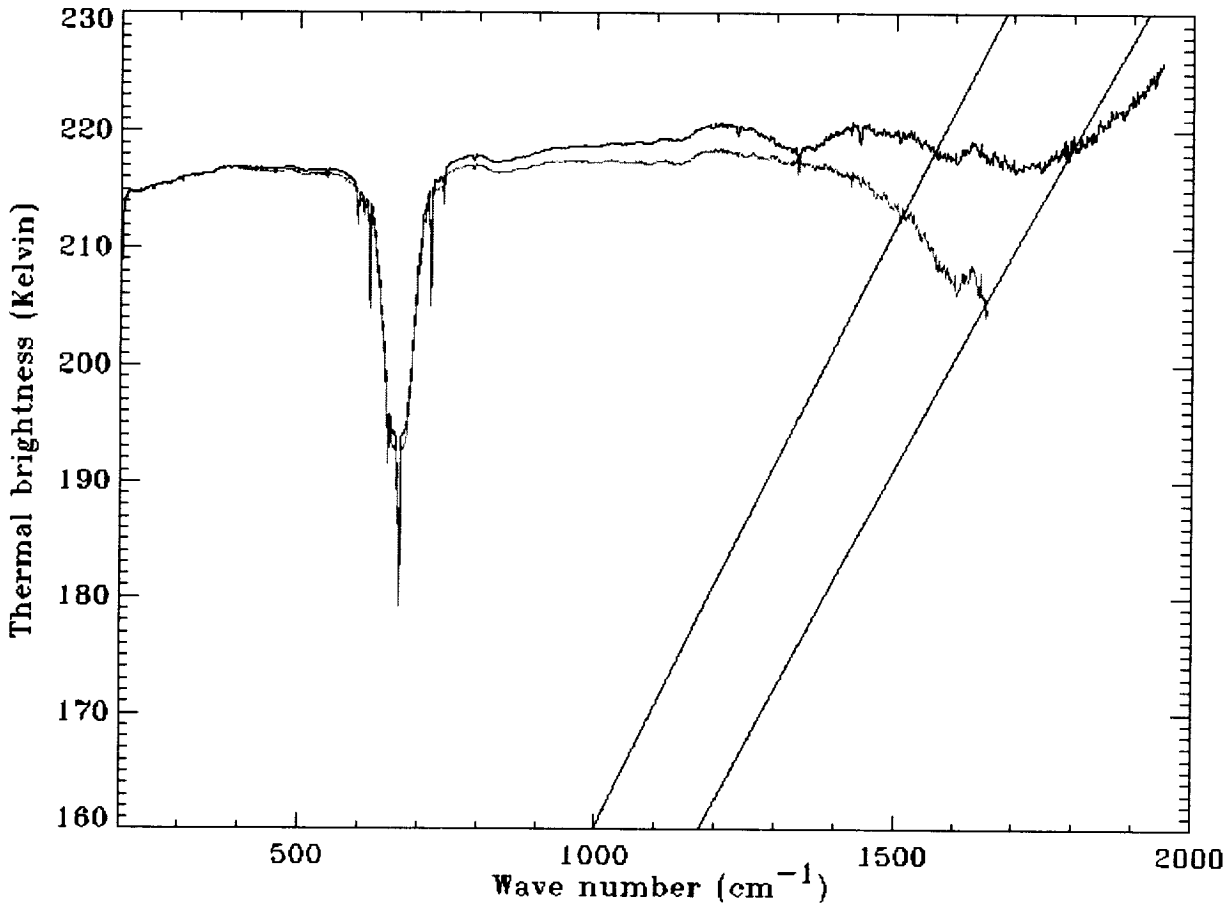

Fig. 1

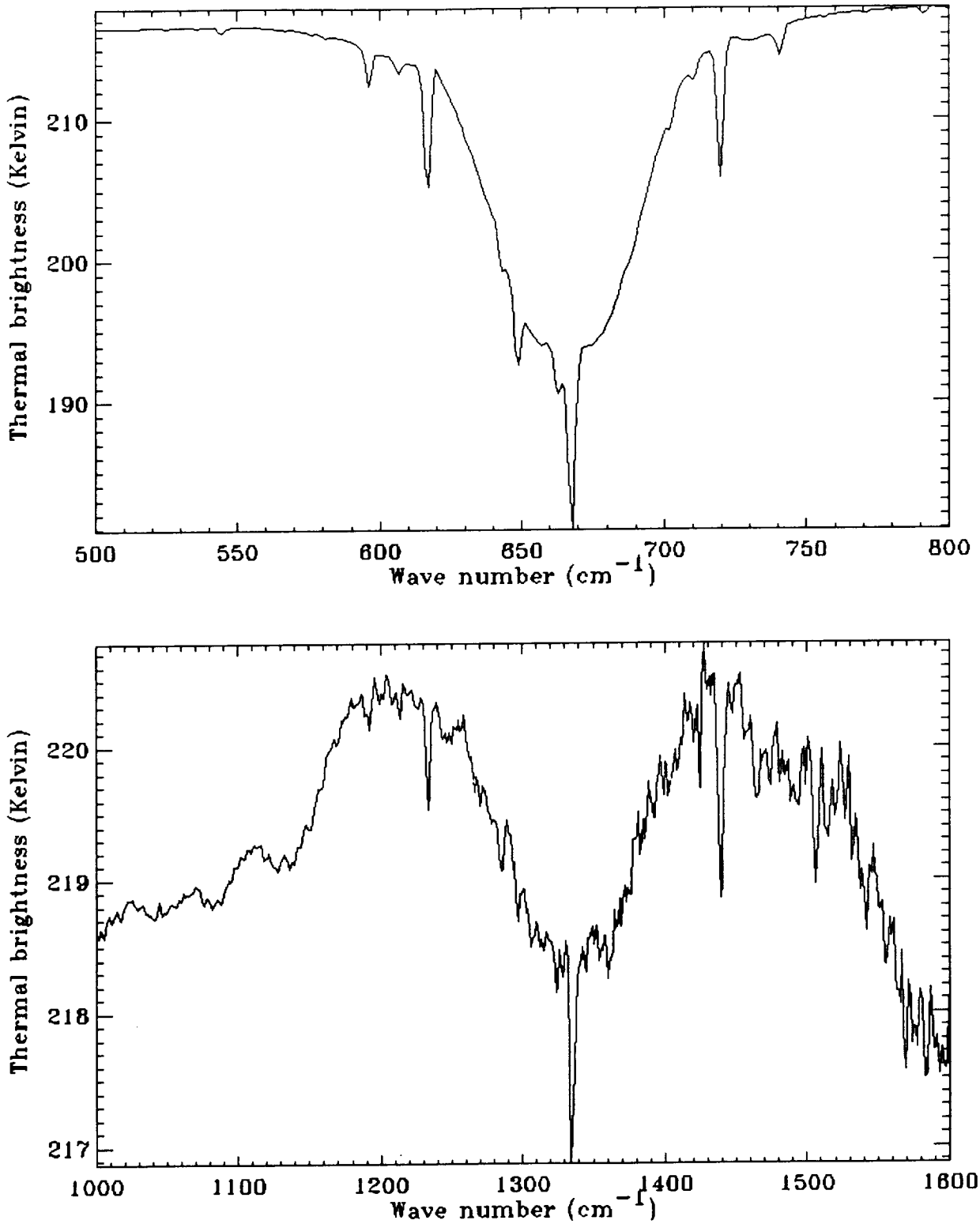
Thermal brightness (Kelvin)
210
200
190
500
550
600
650
700
750
800
Wave number (cm^{-1})
Thermal brightness (Kelvin)
220
219
218
217
1000
1100
1200
1300
1400
1500
1600
Wave number (cm^{-1})

Fig. 2

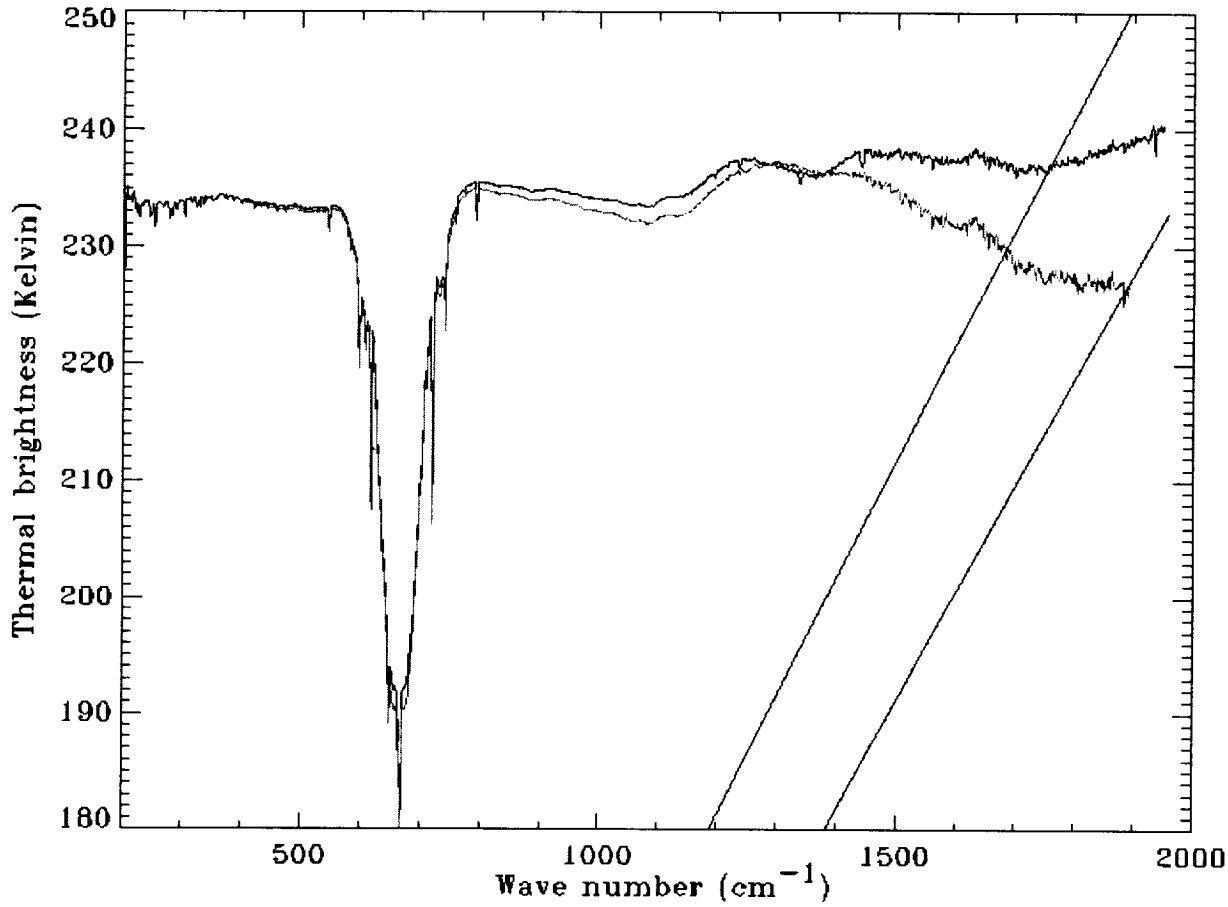
250
240
230
220
210
200
190
180
Thermal brightness (Kelvin)
500
1000
1500
2000
Wave number (cm^{-1})

Fig. 3

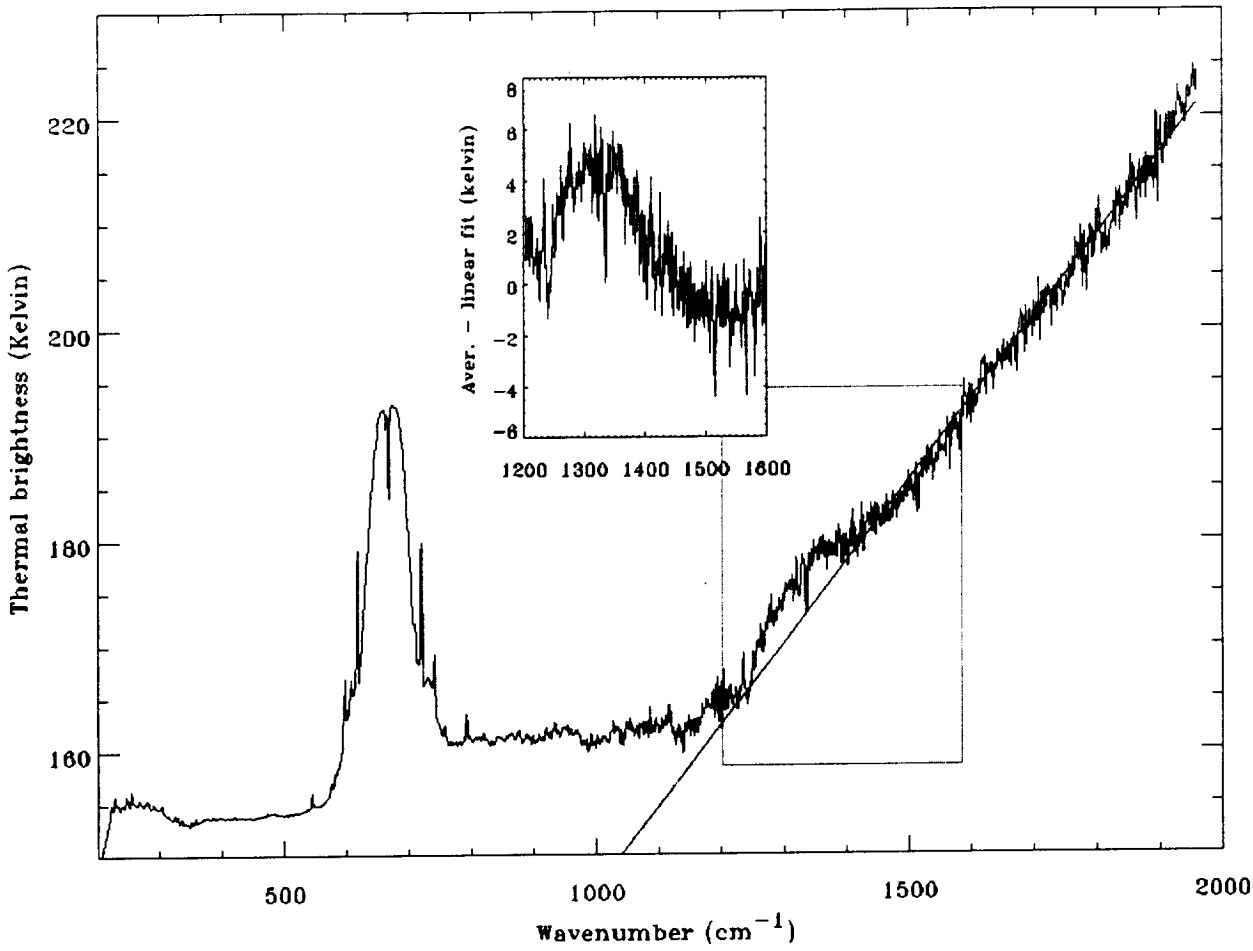
Thermal brightness (Kelvin)
220
200
180
160
500
1000
1500
2000
Wavenumber (cm^{-1})
Aver. - linear fit (kelvin)
8
6
4
2
0
−2
−4
−6
1200 1300 1400 1500 1600

Fig. 4

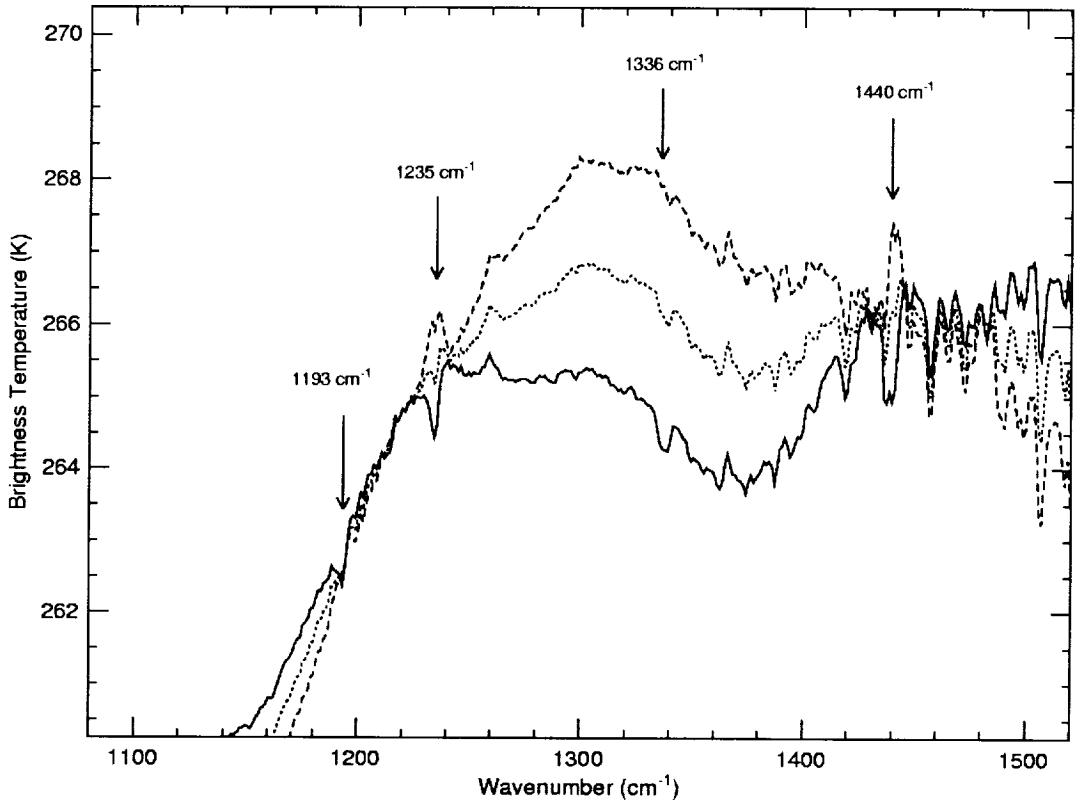
270
268
266
264
262
Brightness Temperature (K)
1100
1200
1300
1400
1500
Wavenumber (cm-1)
1193 cm-1
1235 cm-1
1336 cm-1
1440 cm-1

Fig. 5